



CrossMark
click for updates

Cite this: *RSC Adv.*, 2014, 4, 57087

A green chemistry approach to styrene from ethylbenzene and air on $Mn_xTi_{1-x}O_2$ catalyst†

Sanjay Singh Negi,^a Aswathy Thareparambil Venugopalan,^a Thirumalaiswamy Raja,^{*a} Anand Pal Singh^a and Chinnakonda S. Gopinath^{*ab}

Styrene (ST) is an industrially important commodity chemical, and design of a suitable catalyst, which provides high ethyl benzene (EB) conversion and styrene selectivity at lower temperature with sustainable activity, is one of the major challenges in the field of heterogeneous catalysis. Manganese incorporated in titania ($Mn_xTi_{1-x}O_2$) anatase lattice, prepared via the solution combustion method, was evaluated for oxidative dehydrogenation (ODH) of EB with O_2 or air. $Mn_xTi_{1-x}O_2$ catalysts were characterized by different physicochemical methods. Up to 15% Mn could be introduced into the TiO_2 lattice. TEM and XRD indicate disordered mesoporosity, further confirmed by adsorption isotherm analysis. $Mn_xTi_{1-x}O_2$ catalysts were evaluated for ST synthesis from EB using air or oxygen as oxidant between 440 and 570 °C. Reaction conditions have been varied systematically, such as catalyst composition, and EB/air/ O_2 flow. $Mn_xTi_{1-x}O_2$ shows sustainable 55% styrene yield for 45 h without deactivation under optimum conditions. A thorough analysis of spent catalysts demonstrates the conversion of initial anatase phase $Mn_xTi_{1-x}O_2$ to Mn_3O_4 supported on the rutile (R) phase of TiO_2 . The above change occurs in the first few hours of reaction and the Mn_3O_4 on R- TiO_2 phase is the active phase of the catalyst and responsible for sustainable activity for longer duration.

Received 5th October 2014
Accepted 20th October 2014

DOI: 10.1039/c4ra11814f

www.rsc.org/advances

Introduction

Styrene (ST) is one of the important products in the petrochemical and polymer industries and is a precursor to several resins, plastics, rubbers and other copolymers.¹ Since 1940, the industrial production of ST has been performed through iron oxide promoted by potassium catalysts, by the dehydrogenation of ethylbenzene (EB) with steam, at 700 °C.^{2,3} This dehydrogenation mechanism^{4,5} is endothermic ($\Delta H = 124.9 \text{ kJ mol}^{-1}$) in nature and hence it requires high reaction temperature. Although hydrogen is available as a side product, steam-based processes utilize a large amount of latent heat and they pose thermodynamic limitations.⁶ In addition, coke formation on the catalyst leads to severe catalyst deactivation, and EB conversion of less than 16% was achieved per pass.⁷

Different materials have been used for ST synthesis, such as, metal oxides, carbon. Makkee *et al.* used Al_2O_3 calcined between 500 and 1200 °C, and achieved 42% EB conversion and 87% ST selectivity at 475 °C for 62 h.⁸ Qui *et al.* employed ozonated

multiwalled carbon nanotube (MWCNT) in range of 350–450 °C at atmospheric pressure, O_2 /EB molar ratio varied from 1 : 1 to 3 : 1 with best EB conversion and ST selectivity values of 80% and 92%; however, above high activity occurs at a very low flow rate of 2.3 mL vol% in 55 mL min^{-1} of EB + O_2 + N_2 .⁹ Sekine *et al.* used perovskite and reactions were conducted at 510 or 540 °C at atmospheric pressure in the presence of steam; molar ratio of steam to EB was 2 or 12 with 22% ST yield for 30 min.¹⁰ Venugopal *et al.* has shown ceria containing hydrotalcite at 450 °C at atmospheric pressure a marginally decreasing styrene yield from 47 to 45% over a period of 72 h.¹¹ Shin *et al.* fed a balancing gas of water and EB in helium, over V_2O_5/CeO_2-MgO and achieved EB conversion of 43% and ST selectivity of 91% at 600 °C; prior to the activity measurement, the catalyst was activated in the steam flow of 50 mL min^{-1} by heating up to 650 °C at the rate of 2.5 °C min^{-1} .¹² Sivaranjani *et al.* employed V-doped titania with molecular oxygen at 500 °C and obtained about 50% ST yield initially; however it continuously decreases at higher time on stream.¹³ Various oxidants such as O_2 ,^{13,14} air,¹⁵ N_2O ¹⁶ and CO_2 ¹⁷ have been used, and indeed, air as oxidant is cost effective and preferred green way of oxidation. Above literature reports demonstrates the wide open area of styrene synthesis with better and sustainable yield.

Design of catalysts which are stable, gives high selectivity (>90%) with conversion >50% for EB to ST conversion at lower temperatures around 500 °C or lower is one of the challenges in the field of heterogeneous catalysis.^{8–18} Constant efforts have

^aCatalysis Division, National Chemical Laboratory, Dr Homi Bhabha Road, Pune 411 008, India. E-mail: cs.gopinath@ncl.res.in; Web: <http://nclwebapps.ncl.org.in/csgopinath>; t.raja@ncl.res.in; Fax: +91-20-25902633; Tel: +91-20-25902043; +91-20-25902006

^bCentre of Excellence on Surface Science, National Chemical Laboratory, Dr Homi Bhabha Road, Pune 411 008, India

† Electronic supplementary information (ESI) available: Experimental methods employed and the reactor system (ESI-1). See DOI: 10.1039/c4ra11814f

been made to develop catalysts, operating *via* oxidative dehydrogenation (ODH) mechanism route which is also exothermic in nature¹⁹ to lower operating temperature for EB to ST conversion.^{20,21}

Manganese is known for its superior catalytic properties for various redox processes in heterogeneous catalysis. MnO_x supported on silica have been also used for EB to ST conversion.²² Titania is known as excellent reducible catalytic support, but limited with low surface area. Nonetheless, disordered mesoporous materials²³ with pseudo-three-dimensional (p3D) nature have smaller diffusion lengths^{24,25} thus reactants and products can easily diffuse to and from the active sites of disordered mesoporous materials, which increases the selectivity and yield of the desired product by decreasing the secondary reactions and hence the overall rate of the reaction.

For the present manuscript, we have synthesized large surface area Mn-doped titania (Mn_xTi_{1-x}O₂) catalysts *via* solution combustion method.²⁶⁻²⁹ We used Mn_xTi_{1-x}O₂ materials for EB to ST conversion in a fixed-bed reactor. These catalysts were evaluated between 430 and 570 °C for ST synthesis from ET using air or oxygen as an oxidant. Present disordered mesoporous Mn_xTi_{1-x}O₂ materials exhibits about 57% ST yield with high selectivity (≥95%) under optimized conditions for long durations without undergoing deactivation under reaction condition. The present report is a part of ongoing investigations from our group towards comprehensive understanding of metal oxide catalysts for oxidation and ODH heterogeneous catalytic reactions.³⁰⁻³⁸

Experimental section

Mn_xTi_{1-x}O₂ (x = 0.0–0.15) synthesis by combustion

Disordered mesoporous Mn_xTi_{1-x}O₂ was prepared from cheap chemicals and solution combustion method. All the starting materials were obtained from spectrochem and used as such. Manganese nitrate was used as precursor for manganese and titanyl nitrate for titanium. Solutions were prepared with different manganese to titanium ratio to prepare Mn_xTi_{1-x}O₂ materials with x = 0.01 to 0.15 compositions with 1 : 1 molar ratio of urea to (Mn + Ti). Aqueous solution of precursors in 250 mL beaker was introduced into a furnace pre-heated at 400 °C. Water evaporation followed by combustion generates Mn_xTi_{1-x}O₂ catalysts. Powder catalysts were pelletized and then sieved for 0.8 mm size catalysts particles. Nominal Mn atom percent is given as x in xMT for all materials.

Characterization

Mn_xTi_{1-x}O₂ materials were characterized *via* various physicochemical methods. Routine characterization methods are described in our earlier manuscripts and given in ESI-1.† X-ray photoelectron spectroscopy (XPS) measurements were performed in a laboratory based custom built ambient pressure photoelectron spectrometer (APPEs from Prevac, Poland) under UHV condition.³⁹ XPS measurements were made with Mg Kα X-ray source for X-ray generation and R3000HP (VG Scienta) analyser for energy analysis.⁴⁰

Reaction and reactor system

The catalytic activity was evaluated using a fixed bed continuous flow reactor (FBR) having two furnace zones over a temperature range of 430–570 °C at atmospheric pressure (atm.).^{11,13} An inconel reactor tube with 13 mm internal diameter and 510 mm length was used to pack the catalyst. More detail about reactor system is available in ref. 11 and ESI-1.†

Results and discussion

Structural and textural features

X-ray diffraction. To understand structural features of the materials wide and low angle powder X-ray diffraction (XRD) were recorded for Mn_xTi_{1-x}O₂ materials. XRD results shown in Fig. 1 exhibits diffraction features of 101, 004, 200 and 204 facets of anatase phase of titania present in Mn_xTi_{1-x}O₂ materials. Diffraction pattern is indexed to JCPDS file no.: 21-1272, 21-1276 for anatase phase of titania with small amount of rutile phase. About 2–9 % of rutile phase, (6.2 for TiO₂, 3.8 for MT2, 8.7 for MT5, 5.8 for MT7, 7.9 for MT10, 6.8 for MT12 and 2.1 for MT15) was also observed (# mark in Fig. 1) along with predominant anatase phase in the fresh catalysts. No manganese oxide diffraction peaks were observed up to 15% of Mn content; indicating high dispersion of manganese ions into TiO₂ lattice. Broad peaks indicate the nanocrystalline nature of the catalysts. Crystallite size was calculated using Debye-Scherrer equation for all materials and shown in Table 1. Low angle XRD recorded for all xMT materials show a single broad

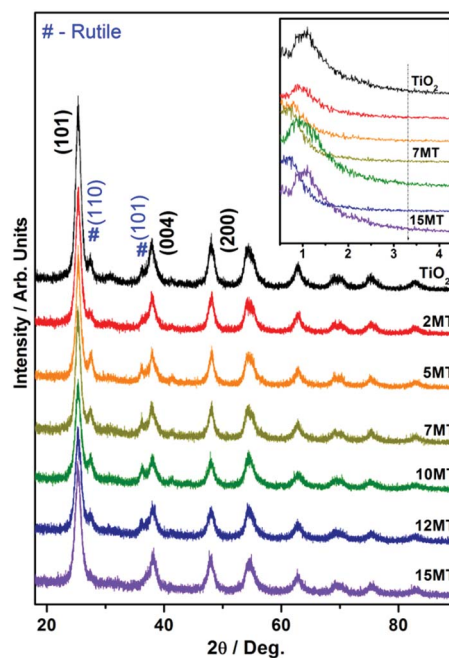


Fig. 1 Wide angle XRD patterns recorded from Mn_xTi_{1-x}O₂ catalysts with different Mn content up to 15 atom%. XRD of TiO₂ prepared by SCM is also shown for comparison. Low angle XRD pattern is given in the inset indicates the disordered mesoporosity.

Table 1 Physicochemical characteristics of $Mn_xTi_{1-x}O_2$

Catalyst ^a	Bulk Mn content	Surface area (m ² g ⁻¹)	Pore size (nm)	Pore volume (cc g ⁻¹)	Crystallite size (nm)
TiO ₂	0	125	3.80	0.2281	8.8
2MT	1.38	79	3.89	0.1121	7.4
5MT	4.10	87	2.25	0.1311	8.5
7MT	6.61	101	3.89	0.1513	8.9
10MT	7.43	110	2.57	0.1811	7.9
12MT	11.04	102	1.87	0.0874	6.8
15MT	14.30	104	2.59	0.1917	7.4

^a x in xMT codes provides Mn atom%.

peak between $2\theta = 0.8$ and 1.3° (Fig. 1 – inset) indicating a disordered mesoporous nature of materials.

TEM. Transmission electron microscopic images recorded are given for representative xMT materials in Fig. 2. TEM images exhibit particles with spherical morphology of 7–8 nm size, with high porosity associated with $Mn_xTi_{1-x}O_2$ materials. It is to be underscored that present set of disordered mesoporous materials were prepared without any surfactant or template molecules, compared to ordered mesoporous materials^{41–43} that employ molecules like P123 copolymer, CTAB *etc.* as surfactant. HRTEM images exhibits d spacing for various planes of TiO₂. Selected area electron diffraction (SAED) patterns were recorded and shows predominantly 101 plane of anatase phases of titania. Similar porous structure was observed for TiO₂, 7MT and 12MT.

SEM-EDAX. Elemental mapping of $Mn_xTi_{1-x}O_2$ materials were studied to understand the distribution of different

elements in the materials. Representative images recorded for different elements from SEM are given in Fig. 3. Manganese and titanium are present and their distribution is shown in yellow and blue colors in separate images, along with the particle image. Homogeneous distribution of Mn in $Mn_xTi_{1-x}O_2$ lattice was observed for all compositions. Mn percentage for all $Mn_xTi_{1-x}O_2$ materials were measured and shown in Table 1.

Nitrogen physisorption. Textural features of xMT materials were studied *via* nitrogen adsorption–desorption isotherms and the results are shown in Fig. 4a; Barrett–Joyner–Hallenda (BJH) pore size distribution plots are shown in Fig. 4b. Mesoporous nature of material can be inferred as all materials show type IV adsorption–desorption isotherm with H₂ hysteresis loop, which is typical of mesoporous materials. Surface area of material was calculated from Brunauer–Emmett–Teller (BET) equation, and shown in Table 1. BJH pore size distribution for xMT materials exhibits bimodal (2MT and 7MT) or unimodal (all compositions except 2MT and 7MT) pore size distribution. xMT materials exhibits average pore diameter of around 3.5 ± 0.5 nm. Calculated pore volume for $Mn_xTi_{1-x}O_2$ materials are also shown in Table 1.

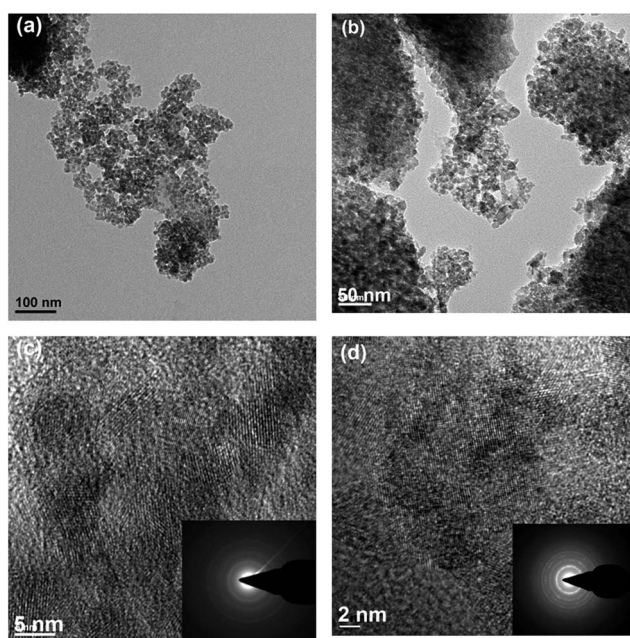


Fig. 2 TEM image of (a) 2MT, (b) 5MT, (c) 10MT and (d) 15MT materials are shown; SAED pattern is shown in inset. Spherical morphology of TiO₂ with (101) facets were found to be predominantly present, for all $Mn_xTi_{1-x}O_2$ materials.

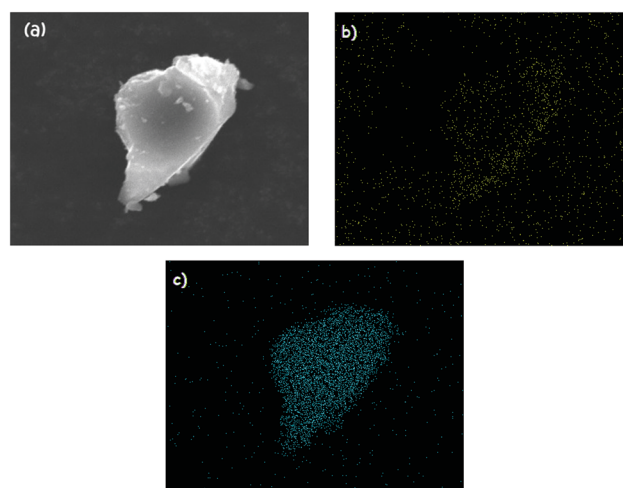


Fig. 3 (a) SEM image of a particle, and the corresponding elemental mapping of (b) Mn in yellow colour, and (c) Ti in blue colour through EDAX analysis on 5MT catalyst. Results indicate an uniform distribution of Mn in titania.

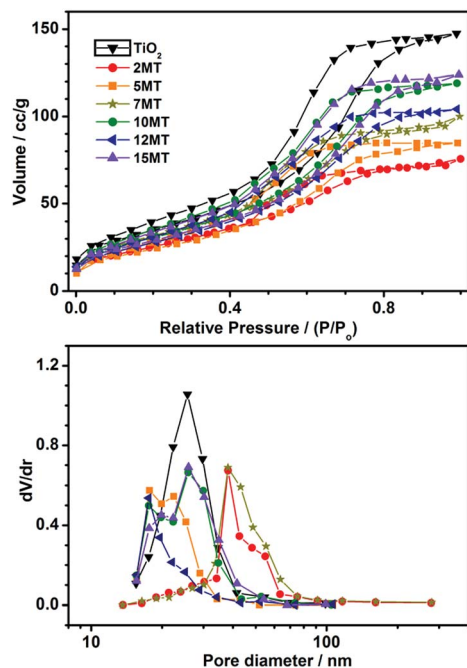


Fig. 4 (a) N₂ adsorption-desorption isotherms, and (b) BJH pore-size distribution of xMT catalysts.

Spectral features

Raman spectroscopy. Raman spectral analysis of xMT materials are shown in Fig. 5. Typical vibrational features of anatase was observed at 145 (E_g), 198 (E_g), 398 (B_{1g}), 516 (A_{1g} + B_{1g}) and 640 (E_g) cm⁻¹. There is shift in position of peak from 145 to 159 cm⁻¹ with an increase in Mn-content in xMT materials. Intensity of all typical features decreased drastically due to Mn incorporation into the titania lattice. The above decrease in the intensity of Raman features is due to the symmetry breaking of Ti-O-Ti by Ti-O-Mn structural features due to incorporation of Mn-ions in TiO₂. XRD and TEM analysis reveals no change in crystallinity and morphology of Mn_xTi_{1-x}O₂ materials compared to that of pure TiO₂. Albeit its small percent of rutile phase (Fig. 1), the same was observed with few compositions prominently (5MT) in Fig. 5.

XPS. Electronic structure of xMT materials was explored *via* X-ray photoelectron spectroscopy of all xMT materials. Fig. 6 shows XPS spectra of Ti2p, and Mn2p (inset) core level spectra of xMT materials. Ti2p_{3/2} core level appears at a binding energy (BE) around 459 eV for all xMT materials. This is in good agreement with the BE reported for Ti⁴⁺ in literature reports.⁴⁴ BE of Mn2p_{3/2} and O1s (not shown) core levels appear around 641.3 ± 0.1 and 529 ± 0.2 eV, respectively, for all Mn_xTi_{1-x}O₂ materials. Observed BE of Mn2p_{3/2} core level around 641.3 eV for all xMT materials indicate the oxidation state of Mn to be 3+.^{45,46} BE of Mn⁴⁺ state was reported to appear at 642.5 eV, which is significantly higher than the BE in XPS spectra, confirming that Mn is not present in 4+ oxidation state in xMT materials. A comparison of ionic sizes of Ti⁴⁺ (0.68 Å), Mn³⁺ (0.645 Å) and Mn⁴⁺ (0.53 Å) also suggest the possibility of Mn³⁺,

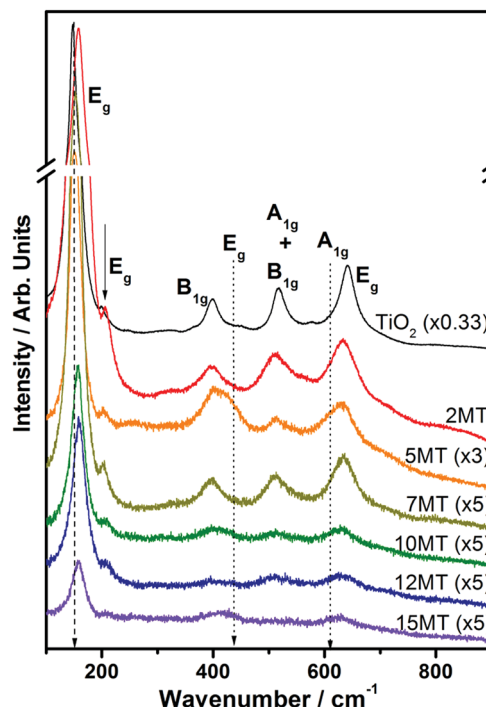


Fig. 5 Raman spectra for xMT materials, multiplied with suitable factors for clarity. No manganese oxide feature was observed up to 15% Mn loading, and broadening of peaks on Mn-doping indicating the symmetry breaking of regular Raman features of anatase phase. Note the blue shift in E_g from 145 on TiO₂ (dashed line) to 159 cm⁻¹ along with line broadening upon Mn introduction into the titania lattice. Rutile phase features are indicated by two dotted arrows.

rather than Mn⁴⁺ oxidation state. Indeed, Mn³⁺ oxidation state is likely to enhance the lattice oxygen storage/release properties under ODH reaction conditions.

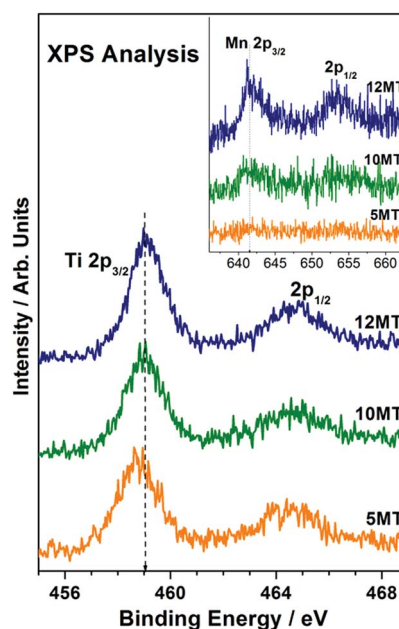


Fig. 6 XPS of Ti2p and Mn2p (inset) core levels of xMT materials.

Catalytic activity

EB to styrene ODH reaction with air or molecular oxygen has been investigated as a probe reaction to explore the catalytic activity of x MT materials. This is primarily to explore the influence of Mn^{3+} introduced in TiO_2 lattice framework. However, caution must be exercised due to the exothermic nature of the reaction with combustible reactant and products in the presence of air or oxygen. Reactions were carried out at relatively low temperature, compared to conventional endothermic reaction,^{4,5} and at atmospheric pressure. Various factors such as flow rates of EB, air/oxygen, catalyst composition and temperature were varied to understand their effects on EB conversion and selectivity to styrene.

Effect of Mn-content. For selective EB conversion to ST, and to minimize the chances of over oxidation of easily combustible EB and ST, active catalytic centres have to be optimized. To find optimum Mn-content for the highest selective oxidation, reactions were carried out with different Mn-content, from TiO_2 to 15 mol% Mn into TiO_2 lattice. Reaction studies were carried out with x MT materials for 12 h on time on stream (TOS) and at EB flow rate of 1.8 mL h^{-1} , and 40 mL min^{-1} O_2 flow at $500\text{ }^\circ\text{C}$. Conversion, selectivity and yield values were measured for different x MT and are plotted in Fig. 7. Except TiO_2 , all x MT catalysts show an increase in ST yield with increase in TOS. TOS data with bare TiO_2 is plotted for reference to underscore the effect of Mn content. TiO_2 exhibited about 20% ST yield, and 72–82% ST selectivity. With increase in Mn-content, EB conversion and ST yield also increased. 15MT shows the best ST yield (55%) and 90–95% styrene selectivity for 12 h, and this catalyst composition shows a sustainable activity for 45 h, which will be discussed later. Although an increase in catalytic activity was observed from TiO_2 to 2MT, with further increasing Mn-content the activity does not increase linearly. 2–10% Mn-doped titania shows comparable yield. This suggests the availability of Mn on the surface is limited due to bulk doping in

titania lattice. However, a comparison of Mn-content to catalytic activity, indicates the decline in specific activity from 2 to 10% Mn, and then it marginally increases at 12 and 15% Mn. We also caution the readers, to take a note on changes in the catalyst nature in the first few hours from anatase phase x MT to Mn_3O_4 supported on rutile titania (*vide infra*). Apart from ST, benzene is a main side product (<5%); toluene and styrene oxide are also formed as minor products with selectivity below 2%. From the above results, it can be inferred that Mn-doped titania centres are the actual catalytic centres for conversion. Selectivity for ST increases with TOS. 12MT, 10MT and 5MT showed gradual increase, 2MT and 7MT showed steady conversion. 15MT exhibits two fold higher yield value than TiO_2 . 15MT catalyst exhibits better yield than intermediate x MT catalysts. 15MT is the best composition among all the compositions that are evaluated. Any further increase in doping of Mn-content resulted in a mixed phase of Mn_3O_4 and $Mn_xTi_{1-x}O_2$ indicating the solid solubility limit of Mn in titania.

Effect of oxygen flow. O_2 supply was optimized to get the highest ST yield and selectivity. EB flow was fixed at 1.8 mL h^{-1} over fixed bed of 15MT catalysts at $500\text{ }^\circ\text{C}$, and O_2 flow was varied at 20, 40 and 60 mL min^{-1} and the reaction was studied. Measured values of conversion, yield and selectivity are plotted for these studies, and the results are shown in Fig. 8. Conversion increased with increase in oxygen flow rates. Styrene yield increased with time due to a gradual increase in EB conversion at 20 mL min^{-1} O_2 flow. O_2 flow at 20 and 40 mL min^{-1} after 6 h show constant conversion values at 35 and 50 mol%, respectively, indicating the steady state attained in 5–6 h. However, 60 mL min^{-1} O_2 flow show a constant yield at 45 mol%; nevertheless, 60 mL min^{-1} O_2 flow shows a steadily declining (increasing) selectivity (conversion). At the end of 12 h, 60 mL min^{-1} O_2 flow exhibits 48% EB yield, and 72% styrene selectivity; in contrast, at 15 h on TOS, conversion decreased to 21% indicating the onset of deactivation (result not shown). EB conversion increases from 25 to 35 mol% with 20 mL min^{-1} O_2

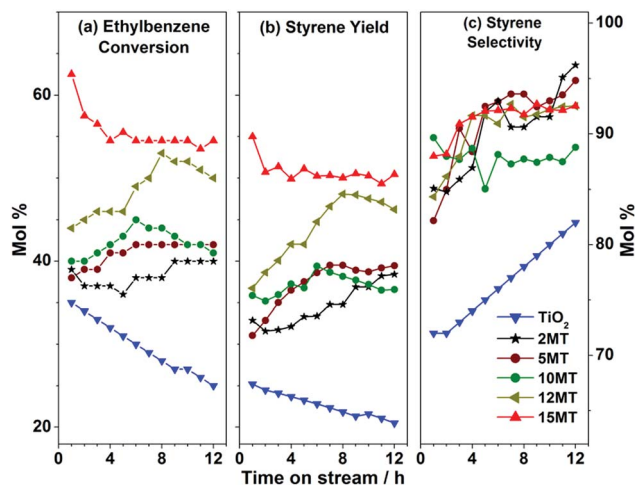


Fig. 7 (a) EB conversion, (b) ST yield and (c) selectivity at $500\text{ }^\circ\text{C}$ are plotted for x MT compositions. Oxygen and EB flow rate was 40 mL min^{-1} and 1.8 mL h^{-1} respectively. 15MT exhibits the highest conversion of EB and yield of ST.

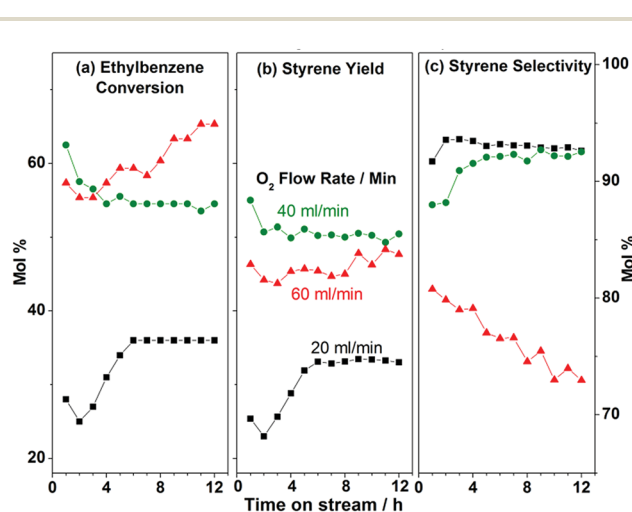


Fig. 8 Effect of oxygen flow on catalytic activity is shown for 20, 40 and 60 mL min^{-1} flow. EB flow rate was maintained at 1.8 mL h^{-1} over fixed bed of 15MT catalysts at $500\text{ }^\circ\text{C}$.

flow in the initial hours indicating a possibility of restructuring of catalyst in the transient state. 40 mL min⁻¹ O₂ flow was observed to an optimum rate for high ST yield. Benzene formed as side product along with toluene and styrene oxide with less than 1% selectivity. It is also to be mentioned that the gas product analysis demonstrating the formation of significant amount of CO₂ suggesting the combustion of reactant and/or product, especially at high oxygen flow (Fig. 8).

Effect of air flow. O₂ was replaced by air to minimize the explosion hazard. Air contains diluted oxygen (21%), and hence a higher flow rate is required to simulate the equivalent amount of oxygen used in the results shown in Fig. 7 and 8. Due to diluted O₂ better activity and ST selectivity was expected. Studies at different air flow rates were carried out to understand the effect of air flow. Air flow at 60, 120, 180 and 240 mL min⁻¹ were carried out at fixed EB flow rate of 1.8 mL h⁻¹ over 15MT at 530 °C, and the results are shown in Fig. 9. With 60 mL min⁻¹ flow there is a steady ST yield at 19%; however, the yield increased steadily at 120 and 180 mL min⁻¹ flows. However, yield decreases at 240 mL min⁻¹, due to facile combustion of EB and ST too, towards CO₂ and water. With increase in flow rates the ST yield increases and the optimum yield was obtained at an air flow rate of 180 mL min⁻¹. 180 mL min⁻¹ air flow exhibit 57% ST yield ≥ 9 h with 95% selectivity. A gradual increase in conversion and yield was observed in the first eight hours of reaction at 120 and 180 mL min⁻¹ flow indicating a possible change in the nature of catalyst. Air flow exhibits higher selectivity for ST compared to O₂ low, always above 95%. Mainly benzene is formed (<3%) as side product.

Temperature dependence. Temperature plays an important parameter for EB to ST conversion. Although EB conversion increases with increase in reaction temperature, above an optimum temperature, combustion is favoured due to favourable oxidizing conditions; this tends to decrease the ST yield. To optimize temperature for ST yield, studies were carried out between 440 and 570 °C at 180 mL min⁻¹ air flow rate.

Measured EB conversion, styrene yield and selectivity values for above reactions are plotted in Fig. 10. Generally conversion increases with increasing reaction temperature. 530 °C shows optimum temperature for EB to ST conversion. The highest ST yield was observed at 530 °C with ST selectivity at 97%. Conversion values increased marginally even up to 12 h for 500 and 530 °C, but steady state was reached at TOS = 5 h at 440 and 470 °C. 570 °C demonstrates a fast increase in conversion up to 8 h, followed by a decline; selectivity was also observed below 90% indicating the increasing contribution from combustion. For all temperatures about 3–5% of side products, such as benzene and toluene are also produced; CO₂ mol% increases from 5 to 10% confirms increasing combustion at higher temperatures (Fig. 10).

Effect of EB flow. Rate of reactant flow over catalyst bed determines the residence time of substrate thus controls catalysts reactivity, and hence overall product distribution. Effect of EB flow rates over 15MT catalysts bed were studied at air flow rate of 180 mL min⁻¹ at 530 °C. To optimize EB flow, different flow rates of 1.2, 1.8, 3.0 and 4.2 mL h⁻¹ were studied, and the results are shown in Fig. 11. 1.2 mL h⁻¹ EB flow shows EB conversion at 38%; however it deteriorates very fast and no conversion was observed at higher TOS, likely due to coke deposition and hence deactivation of the catalyst. TG-DTA analysis further confirms the amount of coke was about 10% (result not shown). 1.8 mL h⁻¹ flow exhibits the highest yield of ST; EB conversion increases gradually between 3 and 9 h, and reaches steady state at 9 h and thereafter the reactivity was maintained. Higher flow rates at 3 and 4.2 mL h⁻¹ shows lower, but steady EB conversion, 97–99% ST selectivity and ST yield for 12 h TOS. ST selectivity observed to be increasing from 90 to 97% at 1.8 mL h⁻¹ EB flow, whereas the same decreases from 90% at 1.2 mL h⁻¹ EB flow. 1.8 mL h⁻¹ flow rate provides optimum EB flow rate for high ST yield.

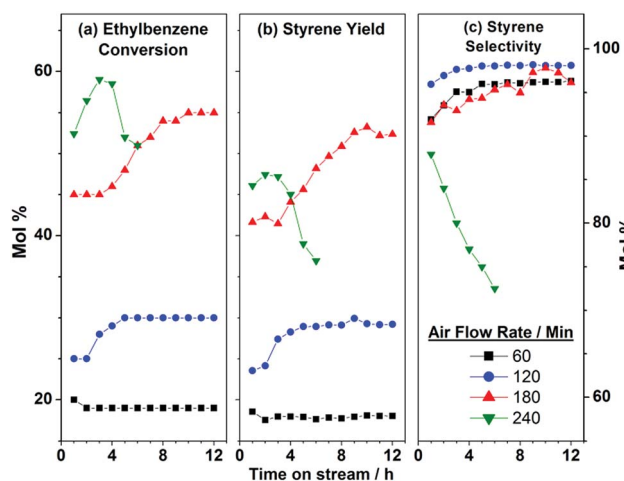


Fig. 9 Air flow rate at 60, 120, 180 and 240 mL min⁻¹ were evaluated. EB at 1.8 mL h⁻¹ and air at 180 mL min⁻¹ flow rate on 15MT catalyst at 530 °C gives highest ST yield.

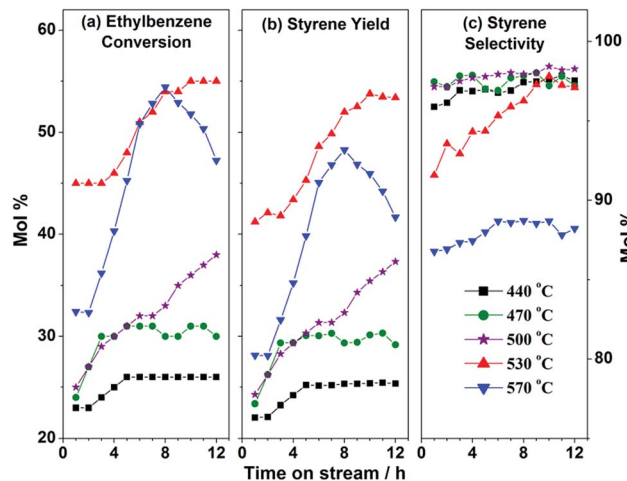


Fig. 10 Effect of reaction temperature on activity trend, at 1.8 mL h⁻¹ EB flow and 180 mL min⁻¹ air flow over 15MT catalysts, between 440 and 570 °C. 530 °C shows the optimum results.

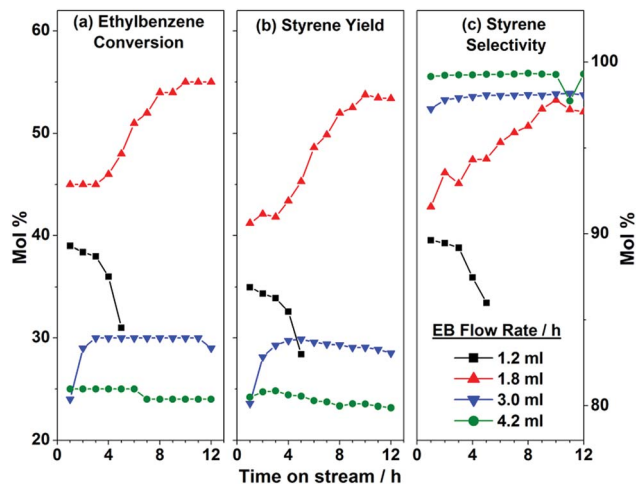


Fig. 11 EB flow rate studied at 1.2, 1.8, 3.0 and 4.2 mL h⁻¹; with optimized air flow at 180 mL min⁻¹ at 530 °C over 15MT catalysts. 1.8 mL h⁻¹ EB flow shows the highest EB conversion and ST yield.

Catalyst stability and reaction sustainability

Optimization studies of reaction parameters for high ST yield were demonstrated earlier and optimum values are 1.8 mL h⁻¹ EB flow, 180 mL min⁻¹ air flow at 530 °C with 15MT catalyst. Possible industrial application of xMT catalyst can be evaluated by subjecting catalytic studies for longer TOS under the above reaction conditions, to ensure robust nature of material and obtaining constant ST yield. 15MT catalysts stability for longer duration (45 h) was studied, and the results are shown in Fig. 12. EB conversion increases from 45 to 58% at 15 h TOS, and thereafter a steady 58% EB conversion was maintained. ST yield also gradually increased from 41 to 55% and afterwards there is no decrease in ST yield up to 45 h thus demonstrating the sustainable nature of catalyst and reaction. Gradual increase in catalyst activity in the first few hours observed under wide variety of reaction conditions demonstrates a change in the nature of catalyst under reaction conditions towards higher active form of the catalyst. Both conversion and selectivity linearly increases, till the reaction reaches a steady state. ST selectivity during whole steady state was observed to be >95%.

Spent catalyst analysis

After reaction, spent catalysts, those are still active and exhibit the high catalytic activity, were collected and analyzed with various physicochemical techniques, such as XRD, Raman spectroscopy, thermogravimetry and differential thermal analysis (TG-DTA), SEM, and TEM. This is mainly to explore the nature of changes that happened to catalysts, especially under transient state conditions which shows an induction period. This is important, since the ODH is known to be an exothermic reaction and local hot spots on the catalyst is likely to occur, which could influence the catalyst.

XRD. Wide angle powder XRD of spent catalysts were analyzed to understand changes in catalysts due to catalytic conversion of EB to ST. For comparison Mn₃O₄ and 5% Mn₃O₄

impregnated on TiO₂ (5% Mn₃O₄/TiO₂) catalysts powder WXR were also recorded and shown in Fig. 13. Narrow and high intense peaks due to rutile phase of TiO₂ at 2θ = 27.5 (110), 36.3 (101), 40.9 (111), 56.8 (211) are observed due to phase change of anatase TiO₂ lattice at reaction temperatures. Mn₃O₄ (JCPDS-ICDD #24-0734) at 2θ = 37.28 and 56.90, and MnO(OH) (JCPDS-ICDD #88-0649) (an intermediate phase of Mn₃O₄), at 2θ = 23.67, 32.21, 35.07, 37.28, 39.17, 40.125, 43.932, 60.7, 64.33, 65.45 and 69.57 are also observed due to precipitation of manganese ions from TiO₂ lattice due to reaction conditions. Spent catalysts exhibit sharp narrow peaks, hinting a growth of large crystallites due to aggregation. Indeed, rutile phase grow at the cost of anatase phase, and the same is observed up to 10% Mn; MT15 shows complete conversion of anatase to rutile phase. Conversion of anatase to thermodynamically stable phase,⁴⁷ underscores the role of exothermic nature of the reaction and its influence in changing the nature of surface and bulk properties of catalyst. Nonetheless, stable catalytic activity observed for 45 h (Fig. 12) suggesting the changes cease to occur under steady state conditions. Thus it can be inferred that catalytic activity is due to Mn₃O₄ and its intermediate MnO(OH) supported over rutile titania.

Raman spectroscopy. Raman spectroscopy analysis of spent xMT catalysts were carried out and the results are shown in Fig. 14. All spent catalysts exhibited a predominant rutile phase along with minor anatase phase features of TiO₂. TiO₂ and 5% Mn₃O₄/TiO₂ catalyst's Raman spectra are given for reference. Spent catalysts exhibits significantly higher intensity compared to fresh catalysts indicating the growth of crystallites to bigger size and hence increase in crystallinity. However, no manganese oxide features appeared in spectra of any catalysts, suggesting a uniform distribution of them on the surface of titania.

TG-DTA. TG-DTA of spent catalysts was measured and the results are shown in Fig. 15. TG plots exhibits weight loss of 1–3% between 200 and 400 °C, and 1–2% weight gain between 500

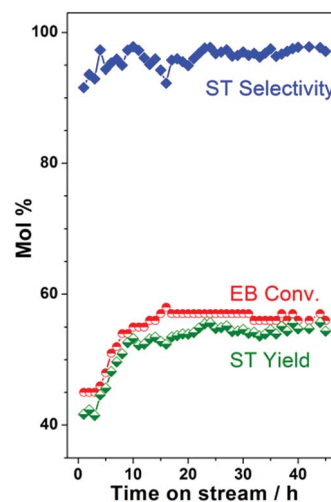


Fig. 12 Catalyst stability was evaluated over 45 h; EB flow at 1.8 mL h⁻¹ with optimized air flow at 180 mL min⁻¹ at 530 °C over 15MT catalyst. Catalyst showed steady ST yield for whole duration without undergoing deactivation.

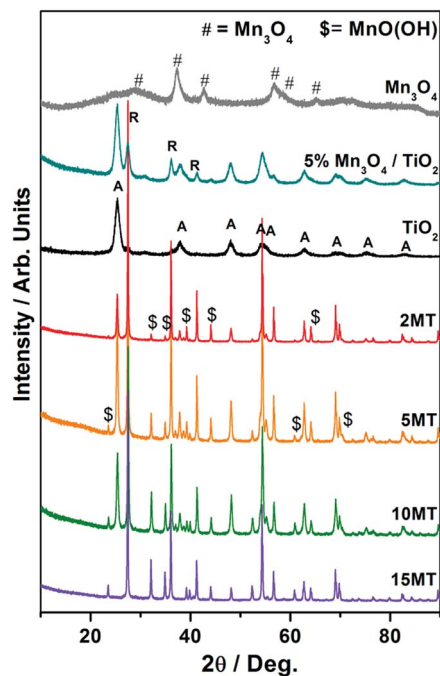


Fig. 13 Powder XRD of spent catalysts and fresh TiO_2 , Mn_3O_4 and 5% $\text{Mn}_3\text{O}_4/\text{TiO}_2$ are shown. Spent catalysts exhibits features of Mn_3O_4 , $\text{MnO}(\text{OH})$ and rutile phase of titania and this is attributed to the exothermic nature of reaction.

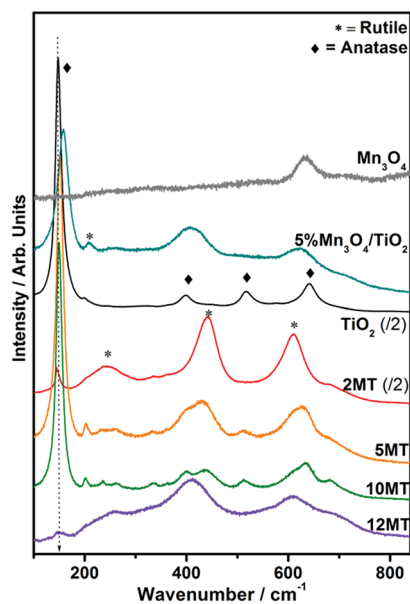


Fig. 14 Raman spectra of spent catalysts exhibits peaks due to anatase and additional rutile phases of TiO_2 supporting XRD results.

and 950 °C; this is in addition to the initial weight loss due to water removal below 200 °C. DTA exhibited exothermic peaks, which are due to carbon burning, that was deposited during catalytic reactions over catalysts surface. MT15 catalysts tested for 45 h shows maximum weight loss, highest peak intensity in DTA results indicating the maximum carbon deposition of 3%

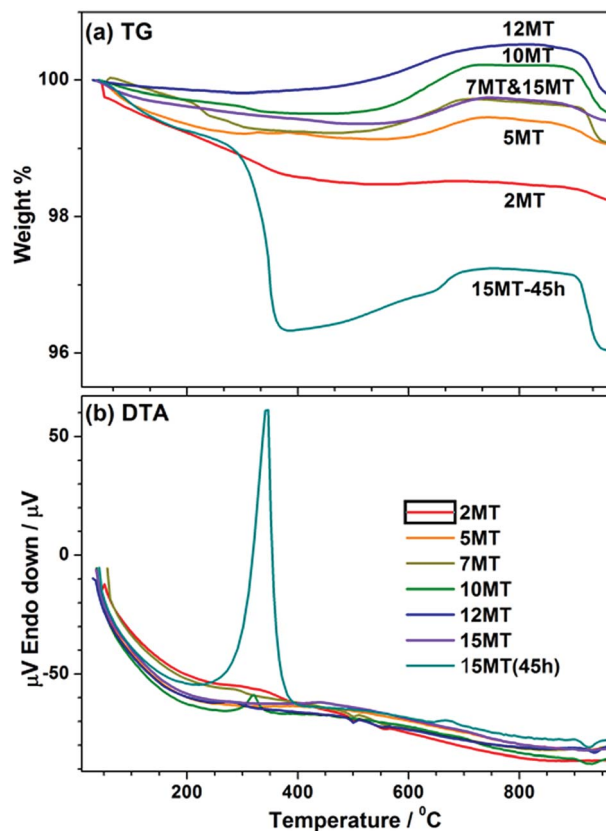


Fig. 15 TG-DTA results for spent catalysts showed exothermic peaks for coke removal up to 400 °C, weight loss followed by weight gain at 700 °C. Catalysts were initially subjected to the following reaction condition at $T = 500$ °C; EB flow rate = 1.8 mL h^{-1} ; oxygen flow rate = 40 mL min^{-1} for 12 h on TOS.

due to reaction. Other compositions tested for 12 h show approximately the similar amount of weight loss in TGA (Fig. 15a). In spite of some coke deposition, sustainable activity observed with 15MT at 530 °C demonstrates the utilisation of air/ O_2 not only towards ODH reaction, but to minimize the coke deposition. Weight gain at high temperatures is attributed to the oxidation of manganese oxides to MnO_2 . Indeed, a systematic increase in weight gain with increasing Mn-content supports the above.

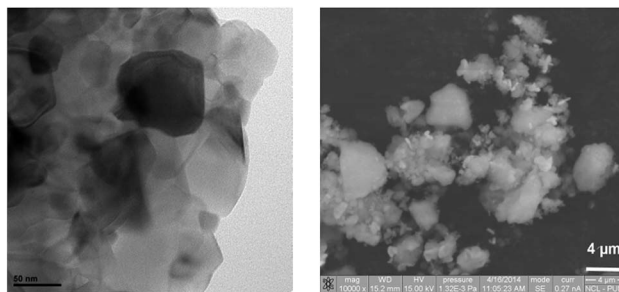


Fig. 16 (a) TEM and (b) SEM image of spent 5MT catalyst. Compared to the TEM results shown in Fig. 2, particle agglomeration is evident. Scale bar length is 50 nm for panel (a).

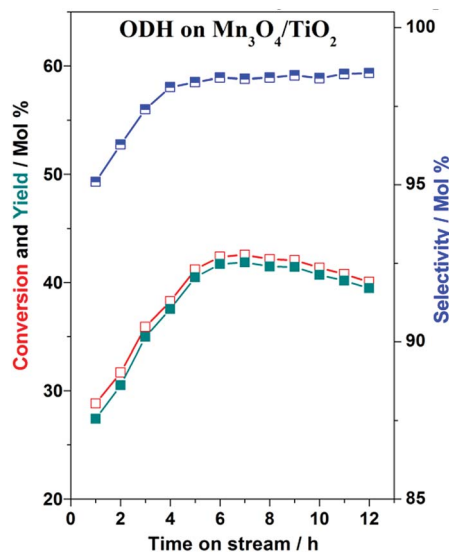


Fig. 17 5% Mn_3O_4 supported on TiO_2 evaluated for EB to ST under optimized condition with air.

SEM and TEM. To understand morphological changes with the catalyst due to reaction, electron microscopy analysis was conducted and the results are shown in Fig. 16. TEM results of spent (5MT) catalyst demonstrate agglomeration to bigger particles, compared to virgin 5MT (Fig. 2b). SEM images show random morphology, with micron size aggregates. TEM and SEM results are further supported by XRD analysis of spent catalysts (Fig. 13) exhibiting sharp peaks due to bigger agglomerated particles of spent catalyst.

ODH with Mn_3O_4 supported on TiO_2 . In view of the above findings with spent catalysts, few control experiments were carried out with Mn_3O_4 supported on anatase phase TiO_2 . Representative result is given in Fig. 17 for 5% Mn_3O_4 loaded on TiO_2 by wet impregnation method and EB to ST conversion was carried out under optimized conditions of 180 mL air per min, EB flow of 1.8 mL h^{-1} at 530°C . Comparable ST yield observed in Fig. 7 for 5MT and Fig. 17 demonstrates the active nature of catalyst is the same in both cases. In fact, the spent catalyst analysis results are in good correlation with that of 5MT results shown in Fig. 13 and 14. It is also to be noted that the change in conversion and selectivity in Fig. 7 and 17 indicates the role of gradual change in interaction between Mn_3O_4 and titania and the conversion of anatase to rutile phase of titania. Although textural properties of nanocrystalline xMT and relatively bigger size particle of Mn_3O_4 on titania varies to a significant extent, they exhibit comparable catalytic activity indicating the minor role of textural properties for the reaction.

Mars–van Krevelen (MvK) mechanism

Kinetics and mechanism of the reaction determines the rate and distribution of products for any catalysis reaction. Different physiochemical and analytical tools helps to understand the above aspects of catalysis. In the present case, the role of lattice oxygen of xMT catalyst was explored by measuring the ODH

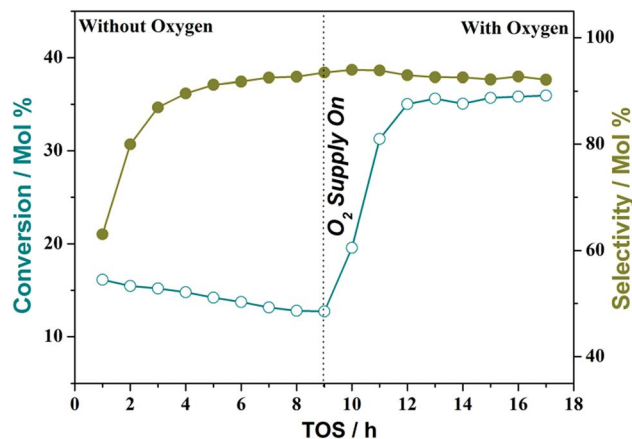


Fig. 18 MT15 catalysts have been tested in absence of air for catalytic reaction at 1.8 mL EB , over 15MT catalyst at 530°C . The MT15 catalysts regained its activity after calcination in oxygen at reaction temperature for 20 min oxygen treatment. 20 mL min^{-1} oxygen flow rate was introduced at $\text{TOS} = 9 \text{ h}$.

reaction in the absence and presence of oxygen/air and a representative result is shown in Fig. 18. Surprisingly, 15MT exhibited catalytic activity of about 15% EB conversion and styrene selectivity of 95%, even in the absence of oxygen/air. A decrease in conversion was observed from the initial 16% conversion to 14% at $\text{TOS} = 8\text{--}9 \text{ h}$. In contrast to the general expectation of steep decline in activity in the first few hours, sustenance of catalytic activity indeed indicates the supply of lattice oxygen towards the ODH reaction. After demonstrating the sustenance of reaction for nine hours, the catalyst was calcined in oxygen (20 mL min^{-1} flow rate) at 530°C , and EB conversion was continued with oxygen flow. An immediate jump in conversion from 14 to 35% in the next three hours, indeed, demonstrates the sustainability of the catalyst system and ODH reaction. Above all, this observation demonstrates the lattice oxygen role in ODH reaction. This clearly indicates xMT catalysts do follow Mars–van Krevelen (MvK) mechanism^{48,49} for EB to ST conversion.

Conclusions

Manganese incorporated in disordered mesoporous nanocrystalline titania catalysts were prepared by simple solution combustion method. $\text{Mn}_x\text{Ti}_{1-x}\text{O}_2$ materials were characterized *via* XRD, Raman spectroscopy, EDX and HRTEM techniques. $\text{Mn}_x\text{Ti}_{1-x}\text{O}_2$ catalysts were evaluated for EB to ST conversion by ODH route. The green chemistry approach using air or O_2 as oxidant was adopted and also it's more economical and safer approach for the conversion. Optimum air flow and EB flow for EB to ST conversion was found to be 180 mL min^{-1} and 1.8 mL h^{-1} , respectively, with 15MT composition exhibiting the highest and sustainable activity at optimum reaction temperature of 530°C . Robust and sustainable nature of the catalyst was demonstrated by activity for 45 h. Conversion temperature is lowered for ST synthesis with high and sustainable yield. Catalyst is stable

and active for long period of time. $Mn_xTi_{1-x}O_2$ materials operate *via* Mars–van Krevelen mechanism as confirmed by catalytic studies in absence/presence of oxygen.

Spent catalyst analysis shows that active phase of catalyst is Mn_3O_4 supported over rutile TiO_2 . Indeed, there is a structural change occurs from anatase to rutile in the first few hours of reaction, due to exothermic nature of reaction. Nonetheless, the sustainable activity observed for 45 h demonstrates the importance of thermodynamically stable rutile phase as support with Mn_3O_4 as the active catalyst. Compared to the systems reported in the literature,^{8–21} Mn_3O_4 supported over rutile TiO_2 is attractive, especially in terms of stability, and yield.

Acknowledgements

S.S.N acknowledges UGC for granting research scholarship. Authors acknowledge the partial financial support from CSC-0404 and CSC-0125 from CSIR, New Delhi under 12FYP.

Notes and references

- M. Chanda and S. K. Roy, *Industrial Polymers, Specialty Polymers and Their Applications*, CRC Press, 2008, p. 305.
- H. A. Wittcoff, B. G. Reuben and J. S. Plotkin, *Industrial Organic Chemicals*, John Wiley and sons, Hoboken, New Jersey, 2013, p. 180.
- H. H. Szmant, *Organic Building Blocks of the Chemical Industry*, John Wiley and sons, 1989, p. 431.
- M. Muhler, J. Schutze, M. Wesemann, T. Raymant, A. Dent, R. Schlögl and G. Ertl, *J. Catal.*, 1990, **126**, 339.
- G. P. Chiusoli and P. M. Maitlis, *Metal-catalysis in industrial organic processes*, 2008, p. 109.
- Y. She, J. Han and Y. H. Ma, *Catal. Today*, 2001, **67**, 43.
- J. C. S. de Araujo, C. B. A. Sousa, A. C. Oliveira, F. N. A. Freire, A. P. Ayala and A. C. Oliveira, *Appl. Catal., A*, 2010, **377**, 55.
- C. Nederlof, V. Zarubina, I. Melian-Cabrera, E. H. J. Heeres, F. Kapteijn and M. Makkee, *Catal. Sci. Technol.*, 2013, **3**, 519.
- N. V. Qui, P. Scholz, T. F. Keller, K. Pollok and B. Ondruschka, *Chem. Eng. Technol.*, 2013, **36**, 300.
- R. Watanabe, M. Ikushima, K. Mukawa, F. Sumomozawa, S. Ogo and Y. Sekine, *Front. Chem.*, 2013, **21**, 1.
- A. K. Venugopal, A. T. Venugopalan, P. Kaliyappan and T. Raja, *Green Chem.*, 2013, **15**, 3259.
- V. K. Nguyen, J. H. Park and C. H. Shin, *Korean J. Chem. Eng.*, 2014, **31**, 582.
- K. Sivaranjani, A. Verma and C. S. Gopinath, *Green Chem.*, 2012, **14**, 461.
- C. Nederlof, V. Zarubina, I. V. M. Cabrera, E. H. J. Heeres, F. Kapteijn and M. Makkee, *Appl. Catal., A*, 2014, **476**, 204.
- N. T. Thao and H. H. Trung, *Catal. Commun.*, 2014, **45**, 153.
- (a) P. Kustrowski, L. Chmielarz, R. Dziembaj, P. Cool and E. F. Vansant, *J. Phys. Chem. A*, 2005, **109**, 330; (b) K. Thirunavukkarasu, K. Thirumoorthy, J. Libuda and C. S. Gopinath, *J. Phys. Chem. B*, 2005, **109**, 13272.
- M. C. Rangel, A. P. M. Monteiro, S. G. Marchetti, S. B. Lima and M. S. Ramos, *J. Mol. Catal. A: Chem.*, 2014, **387**, 147.
- S. S. Negi, K. Sivaranjani, A. P. Singh and C. S. Gopinath, *Appl. Catal., A*, 2013, **452**, 132.
- Q. Wang, X. Li, W. Li and J. Feng, *Catal. Commun.*, 2014, **50**, 21.
- D. Sannino, V. Vaiano and P. Ciambelli, *Res. Chem. Intermed.*, 2013, **39**, 4145.
- N. R. Shiju, M. Anilkumar, S. P. Gokhale, B. S. Rao and C. V. V. Satyanarayana, *Catal. Sci. Technol.*, 2011, **1**, 1262.
- R. Crăciun and N. Dulămită, *Ind. Eng. Chem. Res.*, 1999, **38**, 1357–1363.
- D. G. Kulkarni, A. V. Murugan, A. K. Viswanath and C. S. Gopinath, *J. Nanosci. Nanotechnol.*, 2009, **9**, 371.
- T. Mathew, K. Sivaranjani, E. S. Gnanakumar, Y. Yamada, T. Kobayashi and C. S. Gopinath, *J. Mater. Chem.*, 2012, **22**, 13484.
- K. Sivaranjani, S. RajaAmbal, T. Das, K. Roy, S. Bhattacharyya and C. S. Gopinath, *ChemCatChem*, 2014, **6**, 522.
- M. Mapa and C. S. Gopinath, *Chem. Mater.*, 2009, **21**, 351.
- M. Mapa, K. Sivaranjani, D. S. Bhange, B. Saha, P. Chakraborty, A. K. Viswanath and C. S. Gopinath, *Chem. Mater.*, 2010, **22**, 565.
- M. Mapa, K. S. Thushara, B. Saha, P. Chakraborty, C. M. Janet, R. P. Viswanath, C. M. Nair, K. V. G. K. Murty and C. S. Gopinath, *Chem. Mater.*, 2009, **21**, 2973.
- K. Sivaranjani and C. S. Gopinath, *J. Mater. Chem.*, 2011, **21**, 2639.
- S. Velu, N. Satoh, C. S. Gopinath and K. Suzuki, *Catal. Lett.*, 2002, **82**, 145.
- S. Velu, K. Suzuki and C. S. Gopinath, *J. Phys. Chem. B*, 2002, **106**, 12737.
- M. K. Dongare, V. Ramaswamy, C. S. Gopinath, A. V. Ramaswamy, S. Scheurell, M. Brueckner and E. Kemnitz, *J. Catal.*, 2001, **199**, 209.
- S. Velu, K. Suzuki, M. Vijayaraj, S. Barman and C. S. Gopinath, *Appl. Catal., B*, 2005, **55**, 287.
- N. R. Shiju, M. Anilkumar, S. P. Mirajkar, C. S. Gopinath, C. V. Satyanarayana and B. S. Rao, *J. Catal.*, 2005, **230**, 484.
- T. Mathew, Y. Yamada, A. Ueda, H. Shioyama, T. Kobayashi and C. S. Gopinath, *Appl. Catal., A*, 2006, **300**, 58.
- P. Maity, C. S. Gopinath, S. Bhaduri and G. K. Lahiri, *Green Chem.*, 2009, **11**, 554.
- T. Rajesh, A. K. Rajarajan, C. S. Gopinath and R. N. Devi, *J. Phys. Chem. C*, 2012, **116**, 9526.
- A. C. S. Sekhar, K. Sivaranjani, C. S. Gopinath and C. P. Vinod, *Catal. Today*, 2012, **198**, 92.
- (a) K. Roy, C. P. Vinod and C. S. Gopinath, *J. Phys. Chem. C*, 2013, **117**, 4717; (b) K. Roy and C. S. Gopinath, *Anal. Chem.*, 2014, **86**, 3683.
- P. Devaraji, N. K. Sathu and C. S. Gopinath, *ACS Catal.*, 2014, **4**, 2844.
- N. Maity, P. R. Rajamohanan, S. Ganapathy, C. S. Gopinath, S. Bhaduri and G. K. Lahiri, *J. Phys. Chem. C*, 2008, **112**, 9428.
- A. Lazar, W. R. Thiel and A. P. Singh, *RSC Adv.*, 2014, **4**, 14063.
- E. S. Gnanakumar, J. John, T. Raja and C. S. Gopinath, *J. Nanosci. Nanotechnol.*, 2013, **13**, 2682.

- 44 M. Satish, R. P. Viswanath and C. S. Gopinath, *J. Nanosci. Nanotechnol.*, 2009, **9**, 423.
- 45 S. Bag, K. Roy, C. S. Gopinath and C. Retna Raj, *ACS Appl. Mater. Interfaces*, 2014, **6**, 2692.
- 46 B. Murugan, D. Srinivas, C. S. Gopinath, V. Ramaswamy and A. V. Ramaswamy, *Chem. Mater.*, 2005, **17**, 3983.
- 47 (a) C. S. Gopinath and T. Raja, *J. Phys. Chem. B*, 2001, **105**, 12427; (b) B. Naik, K. M. Parida and C. S. Gopinath, *J. Phys. Chem. C*, 2010, **114**, 19473.
- 48 P. Mars and D. W. van Krevelen, *Chem. Eng. Sci.*, 1954, **3**, 41.
- 49 C. Doornkamp and V. Ponc, *J. Mol. Catal. A: Chem.*, 2000, **162**, 19.